Chapter 4

Franck-Condon blockade beyond sequential tunneling – Cotunneling effects

4.1 Introduction

In this chapter, we go beyond the sequential-tunneling approximation of Chapter 3 and investigate the cotunneling contributions to current and noise in the Franck-Condon (FC) blockade regime. The inclusion of such higher-order processes at strong electron-phonon coupling is motivated by the insight that sequential rates are *exponentially* suppressed in the electron-phonon coupling. By contrast, cotunneling may benefit from the participation of highly excited virtual phonon states with much better overlap, see Fig. 4.1. This increased overlap may render higher-order contributions relevant despite their suppression in powers of the small quantities Γ/k_BT and $\Gamma/\hbar\omega_0$, respectively. The main goal of this chapter consists of answering the pressing question whether and to what degree cotunneling processes modify our previous results for the FC blockade. We find that the low-bias current is indeed dominated by cotunneling contributions, but that the dynamics of self-similar avalanches persists.

One technical difficulty arises when going beyond the order of sequential tunneling, and consists of the apparent divergence of cotunneling rates. This problem can be traced back to the fact that finite-order perturbation theory misses the lifetime broadening of states. Several approaches have been devised to solve this problem [87–89]. Here, we adopt the well-defined and conceptually simple regularization scheme introduced in Refs. [87, 88], which has been detailed in Chapter 2 and Appendix C.

This chapter is organized as follows. For the convenience of the reader not interested in all technical details, we start with a detailed summary of our central results in the following Section 4.2. In Section 4.3 we discuss the cotunneling rates in the blockade regime, and determine their scaling with the electron-phonon coupling. Section 4.4 contains the investigation of cotunneling corrections to the linear conductance and nonlinear current-voltage characteristics. Further insight into the transport mechanism and the fate of avalanches is provided in Section 4.5, where we discuss the current shot noise beyond the sequential-tunneling approximation. Finally, the conclusions from this analysis are summarized in Section 4.6. (Some technical details concerning the calculations are relegated to appendices C, D, G, and I.1.)

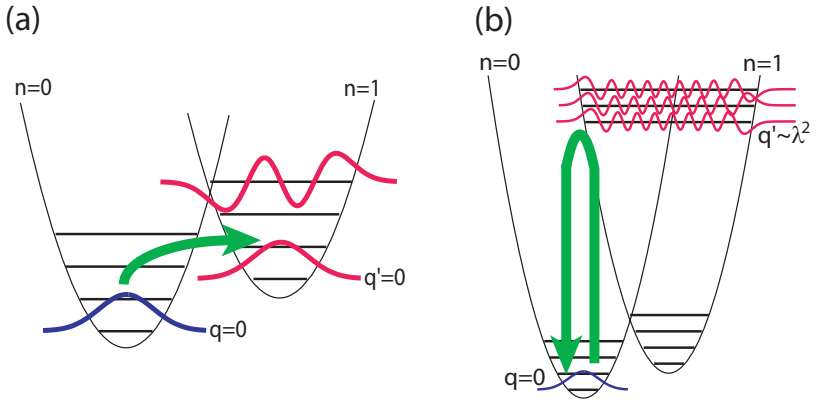

Figure 4.1: (a) Sequential tunneling versus (b) cotunneling for strong electron-phonon coupling. In the FC blockade regime, sequential processes, such as depicted in (a), are strongly suppressed due to the exponentially small overlap of harmonic oscillator wavefunctions. For cotunneling processes (b), this suppression is partly lifted due to contributions from highly excited virtual phonon states.

4.2 Summary of central results

4.2.1 The fate of the FC blockade

The increased overlap of vibrational wavefunctions exploited by cotunneling processes indeed makes cotunneling corrections significant in the FC blockade regime. In contrast to sequential rates, we find that cotunneling rates are not exponentially, but rather algebraically suppressed in the electron-phonon coupling λ, see Eq. (4.1). Consequently, cotunneling dominates the linear conductance for low temperatures over the entire gate-voltage range, see Fig. 4.3. As a result, the paradigm of a gate-controlled crossover between sequential tunneling and cotunneling breaks down for strong electron-phonon coupling, and the linear conductance develops a kink at the degeneracy point. Cotunneling also significantly increases the low-bias current well beyond the linear-response regime, see Fig. 4.5. More importantly however, we find that the remaining strong algebraic suppression of cotunneling rates still leads to a current suppression. Therefore, a central finding is that the FC blockade as such *remains intact*.

4.2.2 Persistence of avalanches and enhanced Fano factors

Another central result is that the avalanche dynamics, found in the sequential-tunneling approximation for weak vibrational relaxation, *persists* in the presence of cotunneling. An intuitive explanation for this is the fact that cotunneling plays a dominant role, whenever the system resides close to the vibrational ground state. However, as soon as an avalanche is initiated, the system reaches highly excited phonon states for which cotunneling becomes irrelevant. Consequently, we find that the inclusion of higher-order processes leads to a coexistence of avalanches and cotunneling, which reduces the Fano factors relative to the sequential-tunneling approximation, see Fig. 4.8. Overall, the persistence of avalanches still leads to Fano factors that are greatly enhanced as compared to the Poissonian limit. Similarly, the power-law behavior in the noise power spectrum remains valid, reduced only

in the frequency range over which it applies, see Fig. 4.9.

4.2.3 Absorption-induced vibrational sidebands

In the case of weak vibrational relaxation, cotunneling also leads to a striking new feature: the appearance of additional vibrational sidebands *inside the Coulomb-blockaded region*, see Fig. 4.6. Inelastic cotunneling provides a unique mechanism for phonon excitations in the Coulomb blockade regime, and for temperatures small compared to the phonon energy. This facilitates the recurrence of sequential processes accompanied by phonon absorption, leading to new vibrational sidebands. Such additional sidebands have previously been observed in experiments with suspended carbon nanotubes [44]. Interestingly, the absorption-induced sidebands are expected to be a generic feature not limited to strong electron-phonon coupling.

4.2.4 Inherent telegraph noise

For strong vibrational relaxation, avalanche dynamics is ruled out and the current noise remains sub-Poissonian in the sequential-tunneling approximation. Surprisingly, we find that cotunneling causes a strong enhancement of current noise at low bias due to inherent current telegraph noise, see Figs. 4.2 and 4.7. Traces of this telegraph behavior are also found for weak vibrational relaxation, rendering this effect robust with respect to the relaxation rate of the system. Its origin is the unusual situation that cotunneling rates are larger than sequential-tunneling rates, $W_{\rm cot} \gg W_{\rm seq}$. Thus, sequential tunneling leads to a slow switching between the two charge states $n = 0$ and 1, which modulates the fast cotunneling dynamics. The cotunneling rates in these two states are different in general, which leads to two distinct current states. This is reflected in large Fano factors $F \sim \Delta W_{\rm cot}/W_{\rm seq} \gg 1$, where $\Delta W_{\rm cot}$ denotes the difference of cotunneling rates in the two charge states.

4.3 Cotunneling rates in the FC blockade regime

The starting point for our investigation is the Anderson-Holstein Hamiltonian, Eqs. (1.1)-(1.3), and we focus on the case of strong Coulomb interaction ($U \to \infty$) throughout this chapter. As explained in Chapter 2 and detailed in Appendix C, the rates for cotunneling processes may be calculated by Fermi's golden rule and subsequently employing the regularization scheme. Here, we discuss the results of this procedure, and the specific behavior of rates for strong electron-phonon coupling.

In the FC blockade regime, the dominant contributions to the cotunneling rates [Eqs. (2.5), (2.6), and (C.11)] arise from highly excited virtual phonon states. According to the Franck-Condon principle, the wavefunction overlap reaches a maximum for transitions that occur (approximately) vertically in the diagram Fig. 4.1(b). For transitions originating in the vibrational ground state $q = 0$, the "optimal" overlap is obtained for states q' of the order of $q' \approx \lambda^2$. Deep inside the FC blockade, the resulting poles $\epsilon \approx \varepsilon_d \pm \lambda^2\hbar\omega_0$, see Eqs. (2.5), (2.6), are typically located well beyond the bias window. As a consequence of that, negative cotunneling rates are essentially irrelevant in the FC blockade regime.[1]

[1]This statement strictly holds for the equilibrated case $\tau \to 0$. For the unequilibrated case $\tau \to \infty$, the

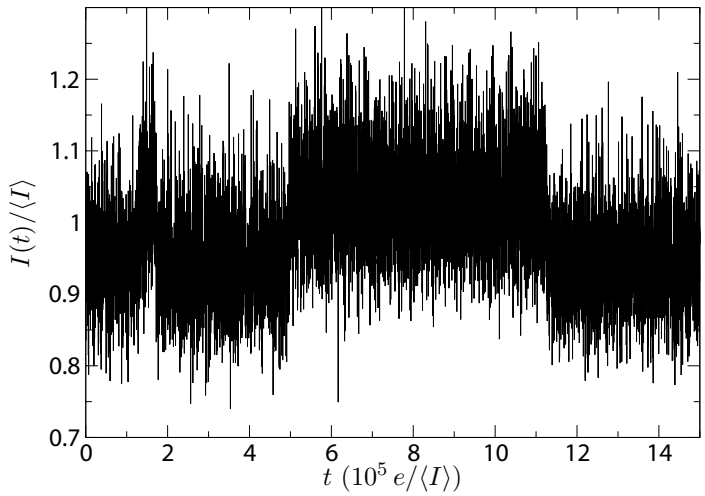

Figure 4.2: Coarse-grained current $I(t)$ as obtained by Monte-Carlo simulation for equilibrated phonons at strong electron-phonon coupling ($\lambda = 5$), with bias and gate voltage fixed to $eV = 0.8\hbar\omega_0$ and $\varepsilon_d = 0.5\hbar\omega_0$, respectively. The time-dependence of the current clearly reveals the current telegraph noise caused by a slow switching between the two molecular charge states via sequential tunneling. ($k_BT = 0.05\hbar\omega_0$, $\Gamma_a = 0.02\hbar\omega_0$; coarse graining over 300 events)

For an understanding of cotunneling rates it is important to note that there is not a single virtual state q'' resulting in maximal overlap, but rather an extended range $\Delta q \sim \lambda$ of excited states centered around $q'' \sim \lambda^2$, see Fig. 4.1(b). By applying Sterling's formula to the expression (2.3) for the FC matrix element $M_{0\lfloor\lambda^2\rfloor}$, we obtain $\left|M_{0\lfloor\lambda^2\rfloor}\right|^4 \approx 1/2\pi\lambda^2$, so that the contribution from the intermediate state $q'' = \lfloor\lambda^2\hbar\omega_0\rfloor$ is given by $\frac{\Gamma_a\Gamma_b}{\pi\hbar}\frac{k_BT+eV}{\lambda^2(\varepsilon_d+\lambda^2\hbar\omega_0)^2}$. Carrying out the coherent sum over the effective range $\Delta q \sim \lambda$, and subsequent squaring leads to an additional factor of λ^2, resulting in the approximation

$$W^{00}_{00;LR} \approx \frac{\Gamma_a\Gamma_b}{\pi\hbar}\frac{k_BT+eV}{(\varepsilon_d+\lambda^2\hbar\omega_0)^2} \tag{4.1}$$

valid for $0 \leq eV \ll \lambda^2\hbar\omega_0$. A more detailed derivation of this expression is given in Appendix H. By contrast to the sequential rates, Eq. (4.1) establishes that cotunneling rates are not exponentially but rather algebraically suppressed. In particular, for $\varepsilon_d = 0$, we have $W^{00}_{00;LR} \sim \lambda^{-4}$.

4.4 Current-voltage characteristics

4.4.1 Linear Conductance

For discrete electronic levels weakly coupled to two electrodes via tunneling junctions, the linear conductance is known to develop peaks whenever an electronic level is aligned with the Fermi energies of the leads. These peaks are well described by sequential-tunneling processes

dynamics within avalanches involving highly excited phonon states may acquire small negative corrections due to cotunneling.

within the rate-equations formalism. Away from the peaks, the sequential-tunneling conductance is exponentially suppressed in the parameter ε_d/k_BT, and cotunneling contributions become important. In the following, we show that strong electron-phonon coupling destroys this gate-controlled crossover between sequential tunneling and cotunneling at low temperatures $k_BT \ll \hbar\omega_0$, rendering cotunneling dominant over wide parameter ranges.

Sequential-tunneling conductance

We start by considering the lowest-order contributions to the conductance, in the limit of low temperatures $\Gamma \ll k_BT \ll \hbar\omega_0$. In this case, only the vibrational ground state is occupied, and any real phonon excitations are negligible. This only leaves the rates W_{00}^{01} and W_{00}^{10} for consideration. Employing the rate-equations approach to this simple situation, the linear conductance for infinite U is obtained as

$$G_{\mathrm{seq}} = -\frac{2e^2}{\hbar}\frac{\Gamma_L\Gamma_R}{\Gamma_L+\Gamma_R}\frac{f'(\varepsilon_d)}{1+f(\varepsilon_d)}e^{-\lambda^2}. \tag{4.2}$$

In the absence of vibrations, this result can be found, e.g., in Ref. [14]. The crucial point here is the fact that the presence of vibrations leads to an exponential suppression of the linear conductance in λ^2, even at the peak value. As discussed in Ref. [14], it is interesting to note that in distinction to the $U = 0$ case, the conductance peak position is not at $\varepsilon_d = 0$ but varies with temperature as $\varepsilon_d = k_BT\ln 2/2$. This shift originates from the fact that the sequential rates $n = 0 \to 1$ are twice as large as the rates $n = 1 \to 0$ due to the spin degeneracy.

Cotunneling conductance

We now consider the next-to-leading order contributions to the conductance. Remaining in the limit of low temperatures $\Gamma \ll k_BT \ll \hbar\omega_0$, the only two additional processes are elastic cotunneling through the empty and the singly-occupied molecule with corresponding rates $W_{00;aa'}^{00}$ and $W_{00;aa'}^{11}$, respectively. The resulting conductance due to elastic cotunneling is given by

$$\begin{aligned} G_{\mathrm{cot}} &= e\frac{\partial}{\partial V}\sum_{n=0,1} P_0^n\left(W_{00;LR}^{nn} - W_{00;RL}^{nn}\right)\Big|_{V=0} \\ &\approx \frac{2e^2}{h}\frac{\Gamma_L\Gamma_R}{1+f(\varepsilon_d)}\left[\frac{1-f(\varepsilon_d)}{(\varepsilon_d+\lambda^2\hbar\omega)^2} + \frac{2f(\varepsilon_d)}{(\varepsilon_d-\lambda^2\hbar\omega)^2}\right]. \end{aligned} \tag{4.3}$$

Here, the apparent poles at $\varepsilon_d = \pm\lambda^2\hbar\omega_0$ are exponentially suppressed due to the Fermi function factors. In fact, they are an irrelevant artefact of our simple approximation in Eq. (4.1). The correct treatment via the regularization procedure eliminates this flaw.

By contrast to the $\sim e^{-\lambda^2}$ suppression of the sequential-tunneling conductance, the cotunneling conductance is only algebraically suppressed as $\sim \lambda^{-4}$. This is a strong indication that, in the regime of strong electron-phonon coupling, cotunneling will dominate the linear conductance, *even at the conductance peak*. Representative numerical results confirming this expectation are shown in Fig. 4.3(a). For $k_BT \ll \hbar\omega_0$, the cotunneling conductance G_{cot} is dominant. In this interesting case, the conductance develops a kink feature at $\varepsilon_d = 0$

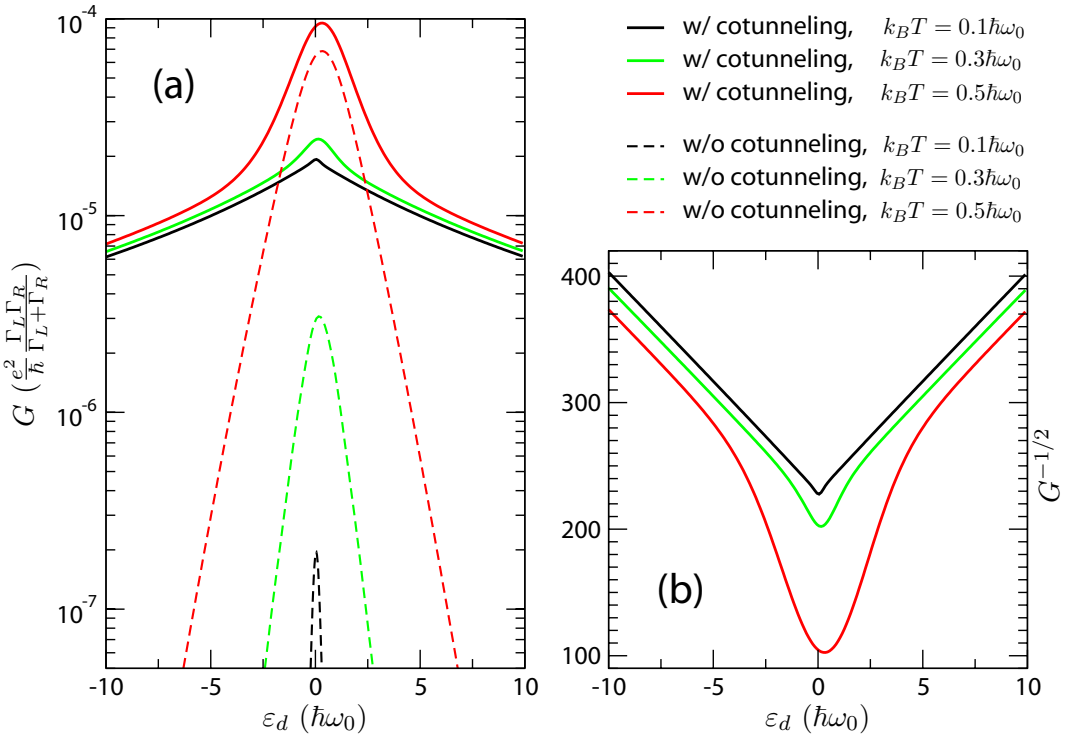

Figure 4.3: Linear conductance as a function of gate voltage in the FC blockade regime ($\lambda = 4$, $\Gamma_a = 0.02\hbar\omega_0$). (a) A comparison of the sequential-tunneling conductance (dashed lines) and the total conductance including cotunneling corrections (solid lines) clearly shows the dominance of cotunneling contributions at low temperatures. At $\varepsilon_d \approx 0$, cotunneling results in a conductance kink for $k_BT \ll \hbar\omega_0$. Sequential contributions become relevant for temperatures $k_BT \gtrsim 0.2\hbar\omega_0$ that allow thermal-induced occupation of excited phonon states. (b) The plot of $G^{-1/2}$ reveals the inverse quadratic decrease of the cotunneling conductance as a function of gate voltage.

broadened over a gate-voltage range given by k_BT, which can be understood from Eq. (4.3). Away from the peak maximum, $G_{\rm cot}$ roughly decays as $\sim(\varepsilon_d+\text{const.})^{-2}$, see Fig. 4.3(b). This is consistent with Eq. (4.3). For larger temperatures $k_BT\gtrsim 0.2\hbar\omega_0$, real excitation of phonons becomes important. Such excitations, which we have neglected in our approximations (4.2) and (4.3), open up additional channels for sequential tunneling. The increase of sequential contributions is evident from the high-temperature curve in Fig. 4.3 (in red color), which shows the recurrence of a sequential-tunneling peak on top of the cotunneling background.

4.4.2 Nonlinear current-voltage characteristics

Sequential current

For strong electron-phonon coupling, we have established in Chapter 3 that the nonlinear IV develops a low-bias gap, essentially eliminating the conventional crossing at the degeneracy point, cf. Fig. 3.1(c). For equilibrated phonons, it is not difficult to estimate the sequential-tunneling current in the FC blockade regime. The main input is that

(i) for low temperatures $k_BT\ll\hbar\omega_0$ and strong relaxation, the initial vibrational state is the phonon ground state $q=0$ for each tunneling processes, and

(ii) the squared Franck-Condon matrix elements $|M_{0q}|^2$ strongly increase with q up to values $q\sim\lambda^2$.

Due to (ii), the current is dominated by tunneling events with maximal change in the phonon number, $\Delta q=\lfloor|eV|/2\hbar\omega_0\rfloor$, as long as $|eV|/2\hbar\omega_0\ll\lambda^2$. Hence, (i) allows us to approximate the current via the rates $W^{01}_{0,\Delta q;\,a}$ as

$$I_{\rm seq}\approx\mathrm{sgn}(V)\frac{e}{\hbar}\frac{2\Gamma_a\Gamma_{a'}}{2\Gamma_a+\Gamma_{a'}}e^{-\lambda^2}\frac{\lambda^{2\Delta q}}{\Delta q!} \tag{4.4}$$

with $(a,a')=(L,R)$ or (R,L) depending on the bias sign. Here, we have assumed $\varepsilon_d=0$ for simplicity, which can in principle always be arranged by adjusting the gate voltage. After averaging over steps, one obtains for voltages larger than temperature

$$I(V)\approx\frac{e}{\hbar}\frac{2\Gamma_a\Gamma_{a'}}{2\Gamma_a+\Gamma_{a'}}\frac{e^{-\lambda^2}\lambda^{|eV|/\hbar\omega-1}}{\Gamma(|eV|/2\hbar\omega+1/2)}\,\mathrm{sgn}(V), \tag{4.5}$$

where the denominator involves the Gamma function $\Gamma(x)$.

The comparison between the asymptotic form Eq. (4.5) and the actual rate-equations solution is depicted in Fig. 4.4. Deviations of the asymptote from the actual solution are observed when the relation $2|eV|\ll\lambda^2\hbar\omega_0$ gradually breaks down. Then, the true current assumes higher values as compared to Eq. (4.5), since assumption (ii) is no longer valid, i.e. not only one but several phonon channels yield significant contributions to the current.

For unequilibrated phonons, where FC blockade leads to self-similar avalanches of electrons (Chapter 3), an estimate for the sequential current is less trivial. The avalanche dynamics makes it necessary to include all phonon channels up to $q\sim\lambda^2$ in a full description. In particular, following the arguments of Section 3.3, the mean electron-number per avalanche as well as the mean number of sub-avalanches within each avalanche will depend on bias and gate voltage, as well as on the coupling strength λ.

Nonlinear IV including cotunneling corrections

We now investigate the cotunneling corrections to the current-voltage characteristics in the FC blockade regime. Representative results for both equilibrated and unequilibrated vibrations are depicted in Figs. 4.5 and 4.6.

We first focus on the case of **equilibrated phonons**. The IV plots for $\varepsilon_d = 0$, Fig. 4.5(a) and (c), illustrate the importance of cotunneling contributions well beyond the linear response regime. Cotunneling corrections significantly increase the current for bias voltages $|eV| < \lambda^2\hbar\omega_0$, the reason being again the increased overlap for oscillator states in cotunneling processes with highly excited intermediate states. It is a crucial point, however, that cotunneling does not lead to a breakdown of the FC blockade. The blockade remains intact, since cotunneling rates are still algebraically suppressed at strong electron-phonon coupling. This suppression remains strong due to the rather large exponents in the scaling with λ, see Eq. (4.1). An additional change caused by the dominance of cotunneling rates is a drastic reduction of step features in the current, see especially Fig. 4.5(c). When plotting the differential conductance dI/dV on a logarithmic scale, see Fig. 4.6, one observes that small steps persist on top of the (much larger) cotunneling background and form the usual system of vibrational sidebands.

An important low-bias feature beyond the sequential-tunneling approximation consists of two steps in dI/dV for $eV = \pm\hbar\omega_0$. These steps mark the onset of inelastic cotunneling. The emergence of such steps is not restricted to the FC blockade, and has been discussed, e.g., in Ref. [59]. Additional steps at bias voltages equal to larger integer multiples of $\hbar\omega_0$ can be observed when going to even lower temperatures than chosen in Figs. 4.5 and 4.6.

For **unequilibrated phonons**, we find that cotunneling corrections again dominate the FC blockade region of the current-voltage characteristics, see Fig. 4.5(b),(d). However, relative to the equilibrated case, the corrections are less drastic. In particular, vibrational steps in IV remain well visible, and the bias range where cotunneling dominates is narrower than in the equilibrated case. This can be explained by the persistence of avalanche dynamics generated by sequential tunneling. Within the FC blockade, important contributions to the current stem from rather featureless cotunneling events. However, phases of pure cotunneling are still interrupted by avalanches. During those, the system attains phonon excitations high enough to make sequential tunneling dominate over cotunneling. Hence, sequential tunneling retains a significant role in the unequilibrated case.

Figure 4.6 demonstrates an additional striking consequence of cotunneling: For unequilibrated phonons, additional vibrational sidebands appear in the Coulomb-blockade region. The mechanism which generates these additional sidebands is the following. The Coulomb-blockade regime, where transport is conventionally dominated by cotunneling, allows for excitation of vibrations through inelastic cotunneling as soon as the bias voltage exceeds the phonon energy. For weak vibrational relaxation, such excitations decay slowly and therefore remain relevant for subsequent tunneling events. The crucial point is that the usual exponential suppression for sequential-tunneling in the Coulomb blockade applies to processes which leave the vibrational state *unchanged*,[2] but not to processes gaining energy through phonon deexcitation. Thus, phonon excitations (induced by inelastic cotunneling)

[2]More generally, the suppression applies to all sequential processes which leave the vibrational state unchanged or increase the excitation level.

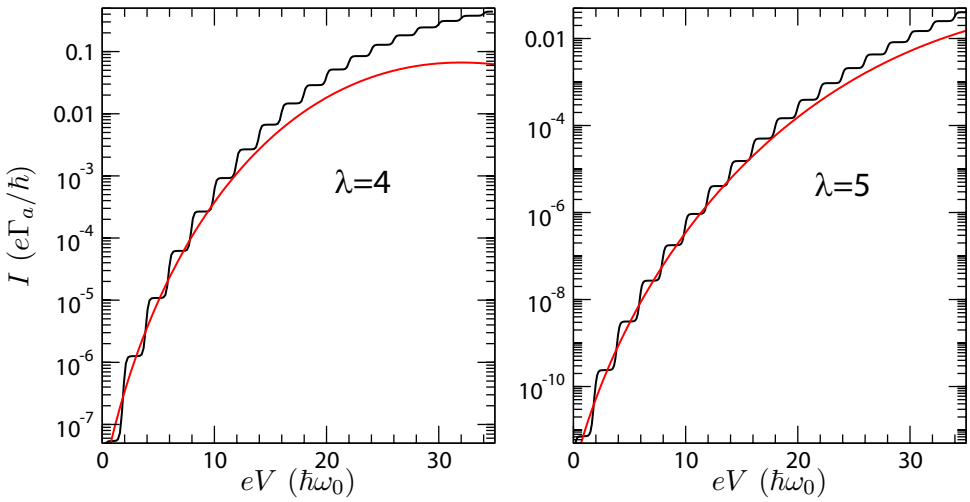

Figure 4.4: Comparison between the sequential-tunneling current (black curve) and the asymptotic formula (4.5) (red curve) for equilibrated phonons in the Franck-Condon blockade regime. ($\varepsilon_d = 0$, $k_BT = 0.05\hbar\omega_0$, $\Gamma_L = \Gamma_R$)

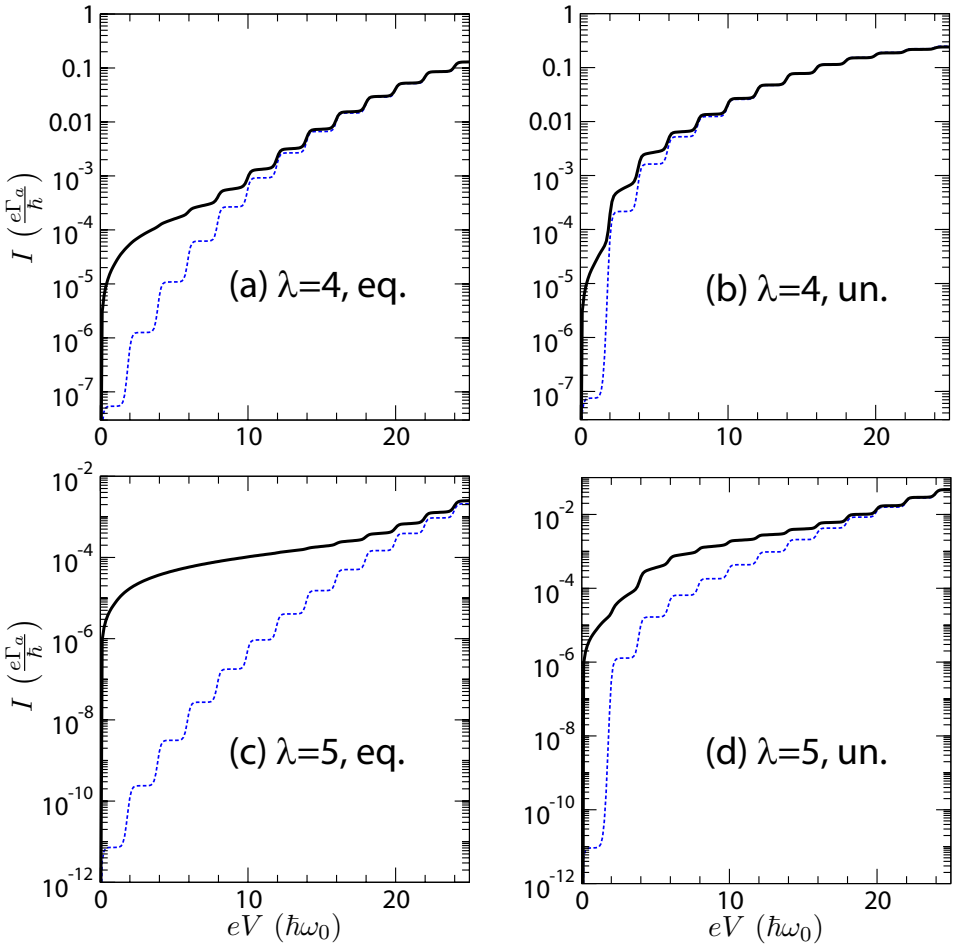

Figure 4.5: Nonlinear current-voltage characteristics in the FC blockade regime. Each graph shows the steady-state current $I^{(1)} + I^{(2)}$ (solid curves), and the sequential current $I^{(1)}$ (dashed curves) for comparison. The electron-phonon coupling and vibrational relaxation strength are chosen as (a) $\lambda = 4$, equilibrated, (b) $\lambda = 4$, unequilibrated, (c) $\lambda = 5$, equilibrated, (d) $\lambda = 5$, unequilibrated. The results unambiguously indicate the dominance of cotunneling contributions in the low-bias FC suppressed regime. (Parameters: $\varepsilon_d = 0$, $k_BT = 0.05\hbar\omega_0$, $\Gamma_a = 0.02\hbar\omega_0$)

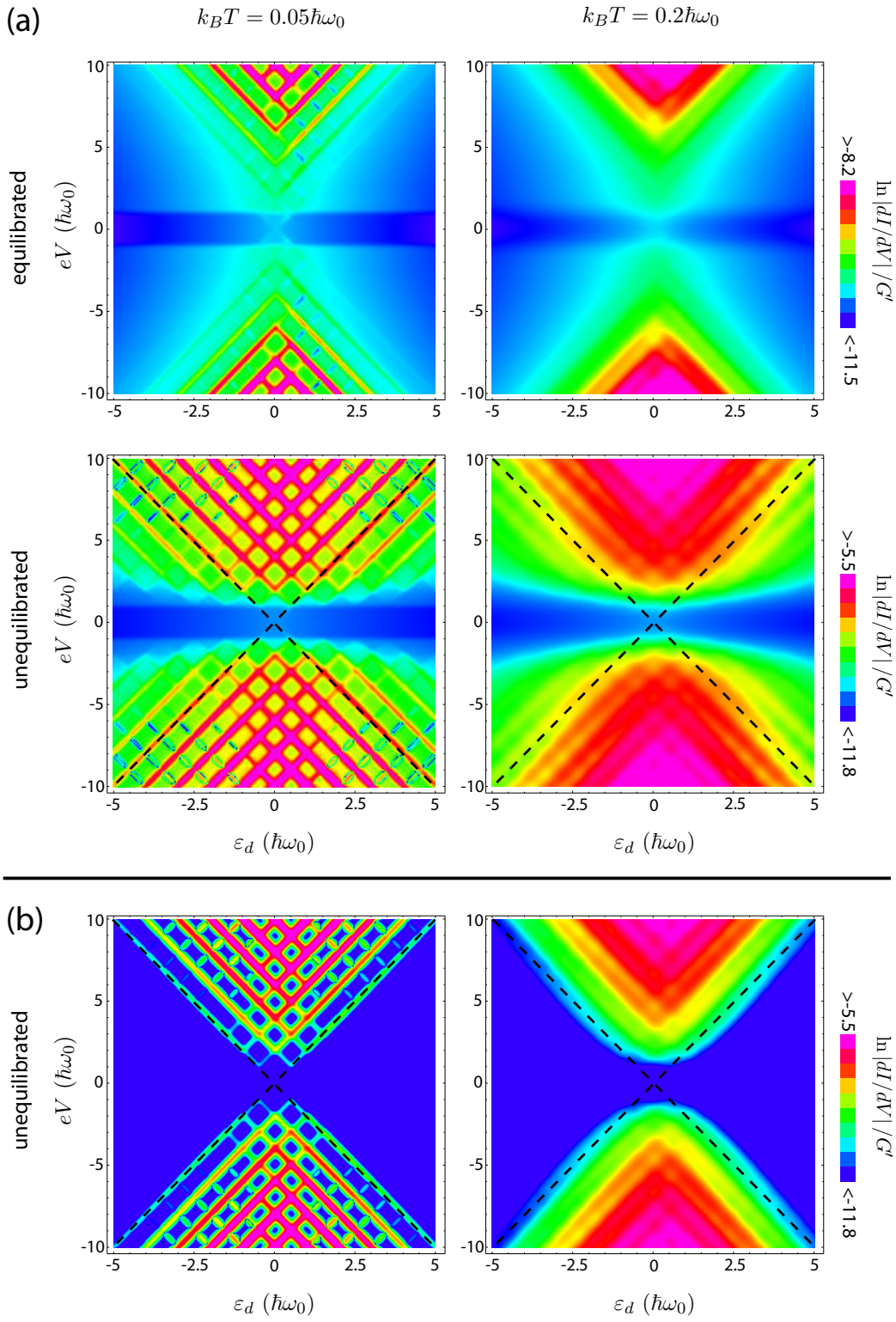

Figure 4.6: (a) Differential conductance dI/dV as a function of gate and bias voltage for $\lambda = 4$ and $\Gamma_a = 0.02\hbar\omega_0$, plotted with a logarithmic color scale. The low temperature plots (left-hand side) show a step in dI/dV due to the onset of cotunneling (horizontal feature at $eV = \pm\hbar\omega_0$). For unequilibrated phonons, inelastic cotunneling gives rise to phonon absorption-induced vibrational sidebands in the Coulomb-blockade regime (whose borders are marked by dashed lines). For comparison, the plots in (b) show the corresponding results within the sequential-tunneling approximation which misses the absorption-induced sidebands. ($G' = \frac{e^2}{\hbar}\frac{\Gamma_L\Gamma_R}{\Gamma_L+\Gamma_R}$)

facilitate the recurrence of sequential tunneling accompanied by phonon deexcitation in the Coulomb-blockaded region. Furthermore, the onset of inelastic cotunneling at $|eV| = \hbar\omega_0$ and the resulting absence of vibrational excitations for lower bias voltages explain why absorption-induced sidebands must terminate at $|eV| = \hbar\omega_0$ and cannot enter the low-bias region.

This interplay between inelastic cotunneling and sequential tunneling results in the observed absorption-induced vibrational sidebands, resembling experimental findings in transport through suspended carbon-nanotubes [44]. We emphasize that the absorption-induced vibrational sidebands are *not* specific to the case of strong electron-phonon coupling, and point out that their presence may be exploited to estimate the vibrational relaxation rate in molecular junctions [44].

Interestingly, phonon excitation due to inelastic cotunneling is the only viable mechanism for absorption-induced vibrational sidebands up to second order in the tunneling. It is crucial to note that thermally induced phonon excitations will in general *not* lead to visible additional sidebands, but rather to a smooth smearing of the Coulomb diamond, see Fig. 4.6(b). This is explained by the fact that vibrational sidebands are clearly visible only for $k_B T \ll \hbar\omega_0$, and in this case thermally activated phonon excitations are negligible.

4.5 Current shot noise

The current shot noise serves as an important tool for acquiring information about the transport dynamics of the system beyond the steady-state current. In particular, we are interested in the Fano factor F and noise spectrum $S(\omega)$ for unequilibrated vibrations to determine the fate of the self-similar avalanches in the presence of cotunneling corrections. We first turn to the regime of strong vibrational relaxation and show that even in this case, cotunneling leads to important new effects.

4.5.1 Zero-frequency noise for equilibrated vibrations – Telegraph noise

As shown in Chapter 3, sequential tunneling results in conventional sub-Poissonian Fano factors for equilibrated phonons, see the dashed curves in Fig. 4.7. Electrons are transferred one by one, interacting with each other only via the charging energy U, which leads to the suppression of F below 1. As depicted in Fig. 4.7 by the black curves, the inclusion of cotunneling processes radically changes this picture. The overall Fano factor remains sub-Poissonian for $\varepsilon_d = 0$. Remarkably, it switches to super-Poissonian behavior for nonzero ε_d in a certain bias range. The magnitude of F strongly depends on the coupling strength λ, as well as gate and bias voltage, and reaches values as large as 100 for $\lambda = 5$.

More insight into this surprising enhancement of noise, which even occurs in the low-bias regime where no phonons can be excited, is obtained by Monte-Carlo simulations. For the parameters of the large maximum of the Fano factor in Fig. 4.7 ($\lambda = 5$, $\varepsilon_d = 0.5\hbar\omega_0$), Fig. 4.2 shows the coarse-grained current as a function of time. This data clearly shows the slow switching between a low and a high current state, on top of much more rapid dynamics within each current state. The underlying reason for this telegraph noise is the role inversion of sequential and cotunneling rates in the FC blockade, i.e. rates for cotunneling are larger than those for sequential tunneling.

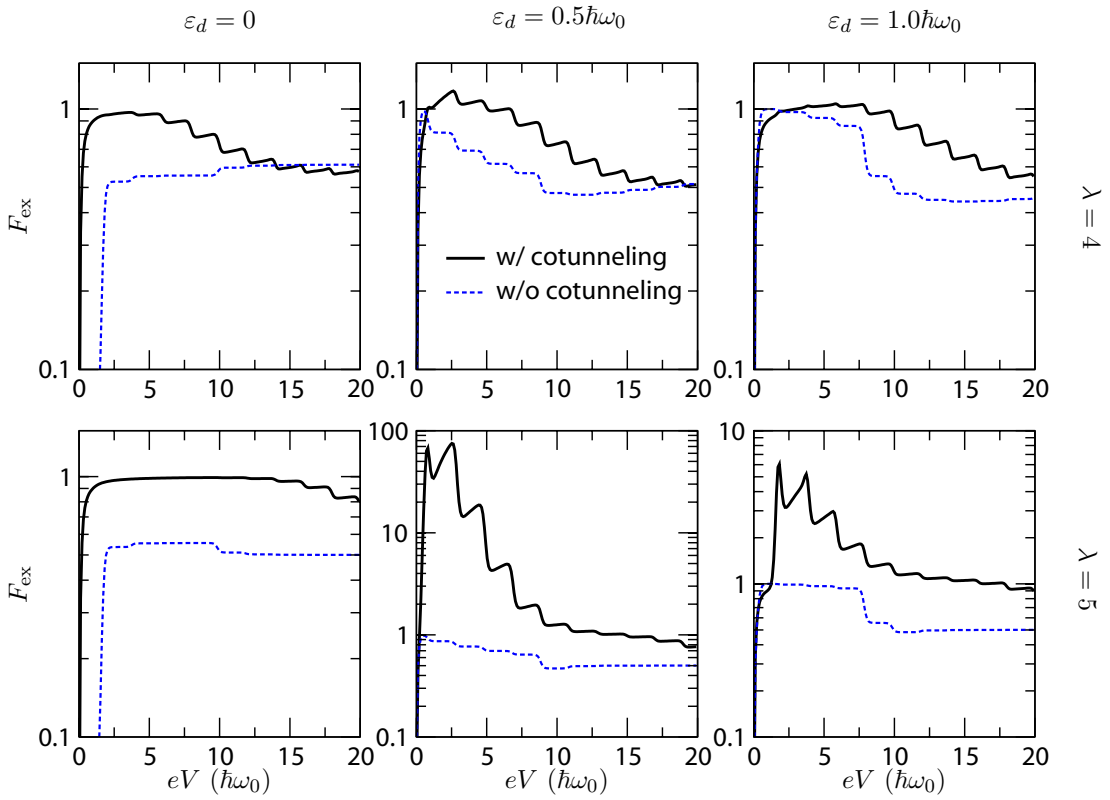

Figure 4.7: Excess noise Fano factor for equilibrated phonons with $\lambda = 4$ (top row) and $\lambda = 5$ (bottom row). For nonzero ε_d we observe large super-Poissonian Fano factors due to current telegraph noise. ($k_BT = 0.05\hbar\omega$, $\Gamma_a = 0.02\hbar\omega$)

In the following, we give a detailed explanation of the telegraph behavior. Denoting the molecular state by $|\,n,q\,\rangle$, a straightforward inspection shows that for $\varepsilon_d = 0.5\hbar\omega_0$ and $eV = 0.8\hbar\omega_0$, the only relevant transitions are (1) $|\,0,0\,\rangle \to |\,1,0\,\rangle$ and $|\,1,0\,\rangle \to |\,0,0\,\rangle$ due to sequential tunneling, and (2) $|\,0,0\,\rangle \to |\,0,0\,\rangle$ and $|\,1,1\,\rangle \to |\,1,1\,\rangle$ due to cotunneling. As explained in Section 4.3, the cotunneling transitions are much faster than the sequential transitions in the FC blockade regime, such that W_{00}^{00}, $W_{00}^{11} \gg W_{00}^{01}$, W_{00}^{10}. The key point in the emergence of the telegraph behavior is the fact that the rates for cotunneling through the empty and through the singly occupied dot are generally different, $W_{00}^{00} \neq W_{00}^{11}$. This can be understood from Eqs. (2.5) and (2.6), noting that ε_d enters the energy denominator with a positive sign for $n = 1$, but with a negative sign for $n = 0$. For $\varepsilon_d = 0$, the two cotunneling rates are identical, and indeed no super-Poissonian noise is detected in this case. However, for nonzero ε_d, the two rates become different. As a consequence, the rapid cotunneling dynamics in the charge states $n = 0, 1$ leads to different mean currents eW_{00}^{00} and eW_{00}^{11}, respectively. The rare sequential transitions facilitate the slow switching between these two current states.

The Fano factor resulting from the current telegraph noise is directly related to the excess charge transmitted in the high-current state during the typical residence time in the corresponding charge state, i.e. $F \sim \Delta W_{\rm cot}/W_{\rm seq}$. Here, $\Delta W_{\rm cot} = \left|W_{00}^{00} - W_{00}^{11}\right|$ denotes the difference of the relevant cotunneling rates. Due to the role inversion of cotunneling and sequential tunneling, we have $W_{\rm cot} \gg W_{\rm seq}$ so that the resulting Fano factor may become large. A more quantitative calculation of the Fano factor can be achieved by employing the generalization of Korotkov's method [84] described in Appendix D. Along these lines, we can derive approximate expressions for the zero-frequency shot noise and its Fano factor,

$$S(f=0) \approx 4e^2 \frac{W_{00}^{01} W_{00}^{10} (W_{00}^{00} - W_{00}^{11})^2}{(W_{00}^{01} + W_{00}^{10})^3}, \tag{4.6}$$

$$F \approx 6 \frac{W_{00}^{01} W_{00}^{10} (W_{00}^{00} - W_{00}^{11})^2}{(W_{00}^{00} + 2W_{00}^{11})(W_{00}^{01} + W_{00}^{10})^3}, \tag{4.7}$$

see Appendix I.1 for details. This approximation is valid whenever W_{00}^{00}, $W_{00}^{11} \gg W_{00}^{01}$, W_{00}^{10} and $W_{00}^{00} \neq W_{00}^{11}$. Counting the orders of cotunneling versus sequential rates in the numerator and denominator of the Fano factor, we find that the Fano factor is indeed of the order of $\Delta W_{\rm cot}/W_{\rm seq}$.

4.5.2 Zero-frequency noise for unequilibrated vibrations – Persistence of avalanches

For unequilibrated vibrations, the sequential-tunneling dynamics in the FC blockade regime is described by self-similar avalanches of electrons, see Chapter 3. The large Fano factors due to sequential tunneling shown in Fig. 4.8 (dashed curves) reflect the large number of electrons per avalanche. In the $\varepsilon_d = 0$ case, the Fano factor is exactly given by $F = 2\langle N_i \rangle$, i.e. twice the mean number of electrons per level-0 avalanche.

The inclusion of cotunneling contributions to the current shot noise results in the black curves depicted in Fig. 4.8. Again, at low biases which do not allow real phonon excitations, we observe traces of telegraph noise. [See the $\lambda = 5$ plots for nonzero ε_d in Fig. 4.8.] For higher biases which facilitate avalanche dynamics, we find that cotunneling generally reduces the Fano factor as compared to pure sequential tunneling. The reason for

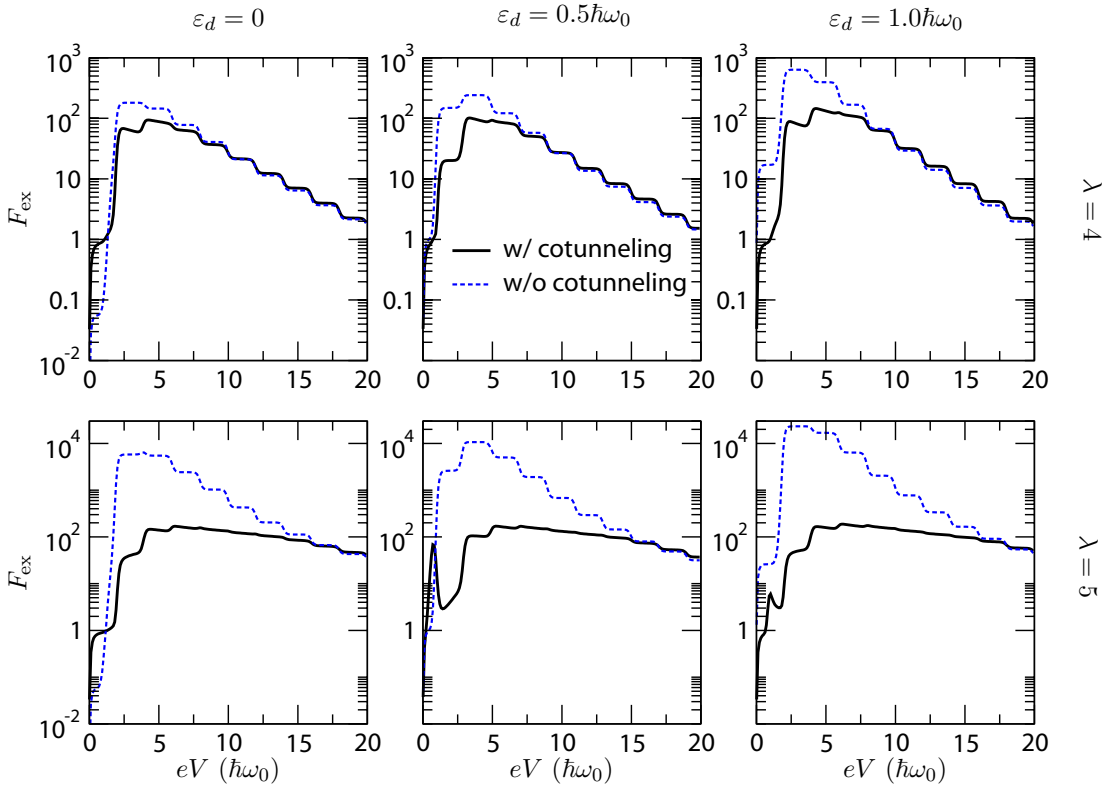

Figure 4.8: Excess noise Fano factor for unequilibrated phonons with $\lambda = 4$ (top row) and $\lambda = 5$ (bottom row) with $k_BT = 0.05\hbar\omega$ and $\Gamma_a = 0.02\hbar\omega$. Due to the coexistence of cotunneling and avalanches, the Fano factor is reduced as compared to the sequential-tunneling approximation. The super-Poissonian peak observed at low bias for $\lambda = 5$ and $\varepsilon_d \neq 0$ signals the occurrence of current telegraph noise.

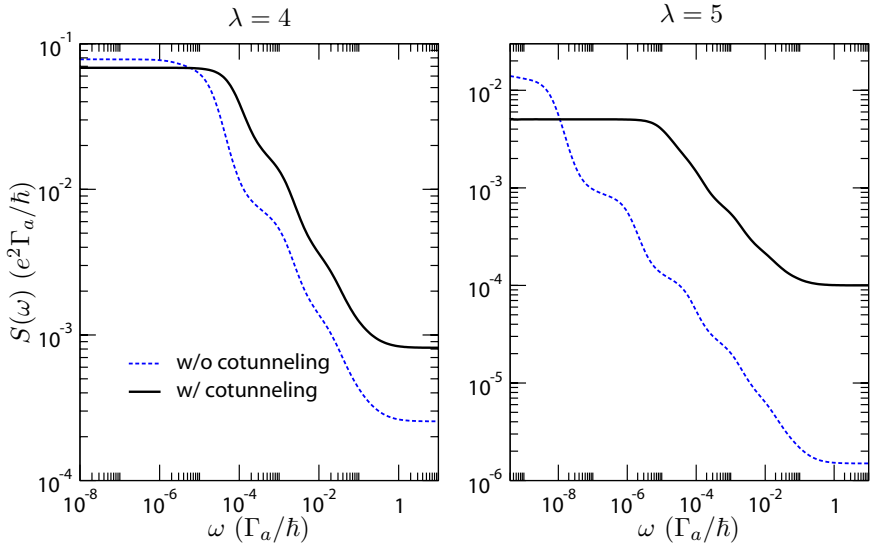

Figure 4.9: (Noise power spectrum for unequilibrated phonons with $\lambda = 4$ (left) and $\lambda = 5$ (right) with $k_BT = 0.05\hbar\omega$, $\Gamma_a = 0.02\hbar\omega$, $\varepsilon_d = 0$, and $eV = 3\hbar\omega$. The approximate power-law behavior reflecting the self-similarity of avalanches persists in the presence of cotunneling. The dominance of cotunneling during sequential waiting times provides a long-time (low-frequency) cutoff for the power law.

this reduction is the coexistence of electron avalanches (leading to large Fano factors) with cotunneling, which results in Fano factors of the order of unity away from the telegraph noise regime. We emphasize that despite the cotunneling-induced noise reduction, the overall Fano factor remains large compared to unity, signalling the persistence of electron bunching in avalanches.

4.5.3 Noise spectrum for unequilibrated vibrations – Self-similarity of avalanches

Probing the self-similarity of avalanches requires one to go beyond the zero-frequency noise. In Chapter 3 we have shown that the characteristic signature of the self-similarity within the sequential-tunneling approximation is an approximate power-law behavior of the noise as a function of frequency ω, $S \sim \omega^{-1/2}$. In Figure 4.9 we present the results for the noise power spectrum including cotunneling corrections.

The central result is that the power-law scaling remains valid. Only the frequency range over which it applies is reduced by cotunneling. In particular, we observe a larger low-frequency cutoff when taking cotunneling into account. This result is consistent with the picture of coexistence of cotunneling and sequential avalanches: In the sequential-tunneling picture, the onset of the power law at low frequencies is essentially given by the strongly suppressed rate for escaping from the vibrational ground state, i.e. $\omega \sim W_{01}^{01/10}$. Going beyond sequential tunneling, we have shown that transitions close to the vibrational ground state are dominated by cotunneling which does not contribute to the avalanche dynamics. Accordingly, the onset of self-similarity and hence the power-law behavior is shifted towards higher phonon levels with corresponding higher rates. This is reflected by a larger low-frequency cutoff for the power law in the noise spectrum.

4.6 Conclusions

We have developed a complete theory of the Franck-Condon blockade in Chapters 3 and 4. This regime, caused by a strong coupling to the bosonic degree of freedom of molecular vibrations, emphasizes the stark contrast between transport through molecular junctions and more conventional nanostructures such as quantum dots. In particular, the intriguing finding that electron-phonon coupling may result in a significant bunching of electrons into a hierarchy of self-similar avalanches dominating the transport, constitutes a novel collective effect unknown from electron transfer through quantum dots.

In distinction to the Coulomb-blockade scenario in quantum dots, where the crossover between sequential tunneling at the conductance peaks and cotunneling away from the peaks may be probed by tuning the gate voltage, we find that the FC blockade regime features the dominance of cotunneling contributions in the entire low-bias region. The underlying reason for this result is the contribution of FC matrix elements to sequential tunneling versus cotunneling: Strong electron-phonon coupling leads to an exponential suppression of these matrix elements relevant for low-bias sequential tunneling. By contrast, cotunneling involves highly excited, virtual phonon states with much better overlap, resulting in a mere algebraic suppression of cotunneling rates. We have shown that the FC blockade and avalanche-type transport persist despite the cotunneling corrections. Furthermore, we

have established that cotunneling leads to a number of remarkable effects missed by the sequential-tunneling approximation. In summary, our central results are:

- Cotunneling dominates the linear conductance and low-bias current-voltage characteristics, yet leaving the Franck-Condon blockade intact.
- Instead of a peak, the linear conductance exhibits a cotunneling kink at the degeneracy point of the two molecular charge states.
- Apart from horizontal dI/dV steps due to inelastic cotunneling, the most important consequence of cotunneling is the appearance of additional absorption-induced vibrational sidebands inside the Coulomb-blockade regime, relevant for unequilibrated vibrations.
- The role inversion between cotunneling and sequential tunneling may cause current telegraph noise whenever the electronic level is not centered between the left and right Fermi energy. This is reflected in strongly enhanced Fano factors, independent of the vibrational relaxation strength.
- Current noise results for the unequilibrated regime establish that the self-similar avalanche transport persists in the presence of cotunneling. In particular, the zero-frequency shot noise maintains super-Poissonian Fano factors large compared to unity, indicating that the bunching of electrons in avalanches remains important. Furthermore, the characteristic power-law behavior of the noise spectrum was shown to remain valid when including cotunneling corrections, signalling the self-similar structure of avalanches.

For a more detailed account of results we refer the reader to Section 4.2. In closing, we emphasize the appeal of realizing shot noise measurements in experiments with single-molecule devices. These could provide essential information about the transport mode, which cannot be accessed by current-voltage characteristics. Experimental efforts in this direction are under way in several research groups.